

Accepted Manuscript

Investigation of charges-driven interaction between graphene and different SiO₂ surfaces

Maria F. Pantano, Erica Iacob, Antonino Picciotto, Benno Margesin, Alba Centeno, Amaia Zurutuza, Costas Galiotis, Nicola M. Pugno, Giorgio Speranza

PII: S0008-6223(19)30295-7

DOI: <https://doi.org/10.1016/j.carbon.2019.03.071>

Reference: CARBON 14062

To appear in: *Carbon*

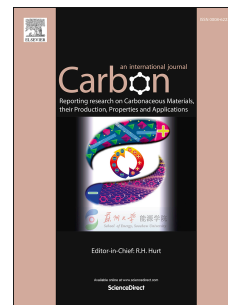
Received Date: 11 February 2019

Revised Date: 14 March 2019

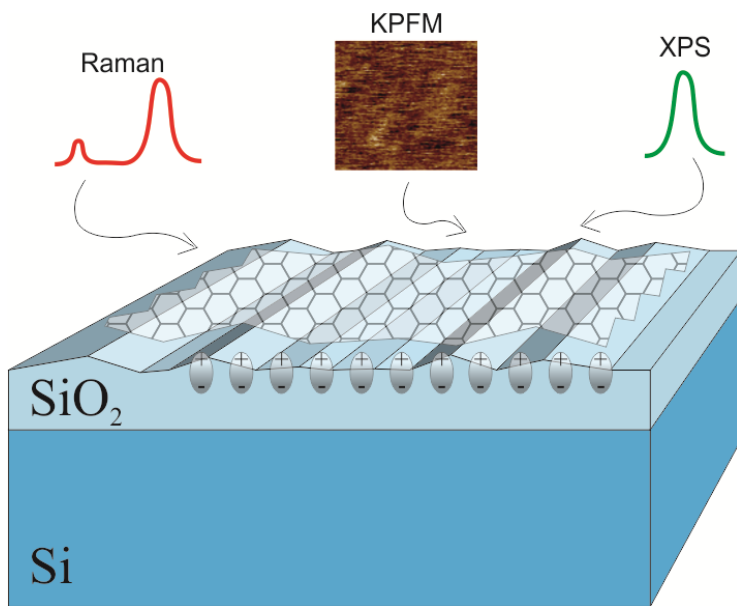
Accepted Date: 21 March 2019

Please cite this article as: M.F. Pantano, E. Iacob, A. Picciotto, B. Margesin, A. Centeno, A. Zurutuza, C. Galiotis, N.M. Pugno, G. Speranza, Investigation of charges-driven interaction between graphene and different SiO₂ surfaces, *Carbon* (2019), doi: <https://doi.org/10.1016/j.carbon.2019.03.071>.

This is a PDF file of an unedited manuscript that has been accepted for publication. As a service to our customers we are providing this early version of the manuscript. The manuscript will undergo copyediting, typesetting, and review of the resulting proof before it is published in its final form. Please note that during the production process errors may be discovered which could affect the content, and all legal disclaimers that apply to the journal pertain.



Graphical Abstract



ACCEPTED MANUSCRIPT

Investigation of charges-driven interaction between graphene and different SiO₂ surfaces

Maria F. Pantano¹, Erica Iacob², Antonino Picciotto², Benno Margesin², Alba Centeno³, Amaia Zurutuza³, Costas Galiotis^{4,5}, Nicola M. Pugno^{1,6,7}, Giorgio Speranza^{2,8,9*}*

¹Laboratory of Bio-inspired & Graphene Nanomechanics, Department of Civil, Environmental and Mechanical Engineering, University of Trento, Via Mesiano 77, 38123 Trento, Italy

²Centre for Materials and Microsystems, Fondazione Bruno Kessler, Via Sommarive 18, 38123 Povo (TN), Italy

³GRAPHENEA S.A. Paseo Mikeletegi 83, 20009, San Sebastian, Spain

⁴Institute of Chemical Engineering Sciences, Foundation for Research and Technology – Hellas (FORTH/ICE-HT), Patras 265 04, Greece

⁵Department of Chemical Engineering, University of Patras, Patras 26504, Greece

⁶School of Engineering and Materials Science, Queen Mary University of London, Mile End Road, London E1 4NS, U.K.

⁷Ket-Lab, Edoardo Amaldi Foundation, Italian Space Agency, Via del Politecnico snc, 00133 Rome, Italy

⁸Istituto Fotonica e Nanotecnologie – CNR, via alla cascata 56, 38123 Trento, Italy

⁹Department of Material Engineering, University of Trento, Via Mesiano 77, 38123 Trento, Italy

* nicola.pugno@unitn.it;

* speranza@fbk.eu

Abstract. As being only one atom thick, most of the device applications require graphene to be partially or fully supported by a substrate, which is typically silicon dioxide (SiO_2). According to a common understanding, graphene interacts with SiO_2 through weak, long-range van der Waals forces emerging between instantaneous/induced dipoles, in contrast to the experimental evidence that reveals a surprisingly high interaction between graphene and SiO_2 . In order to get further insight into this phenomenon, we carried out diverse physical measurements on SiO_2 substrates, prepared via different fabrication protocols, with and without graphene on top. As a result, the role of the oxide surface charges is recognized for the first time as a main factor causing graphene to strongly interact with SiO_2 . Our findings provide guidelines for designing 2D materials interaction with a substrate through modulation of surface charges. This, in turn, can facilitate the development of new graphene based microelectronic devices.

Keywords: Graphene, Silicon oxide, Surface charges, Electrostatic interaction, SKPM, Raman spectroscopy, XPS

1. Introduction

As the performances of silicon-based electronics increase with dimensional scaling, graphene has been receiving increasing attention by the scientific community. Owing to its exceptional electronic properties that arise from the high electron mobility of carbon atoms confined in a single layer, it is likely that graphene will take a pivotal role in the future of microelectronics [1], [2], [3], [4]. Unfortunately, graphene electrical properties are very sensitive to the interactions with the external environment. In fact, previous theoretical studies showed that the electronic states near Dirac points can be influenced by the absorption of some molecules [5],[6], structural corrugation [7], defects [8] and the interaction with a substrate [9], [10]. This latter condition occurs frequently in many applications. For example, graphene is commonly found as deposited onto a substrate in novel electrical switches [11], surface coatings for lubrication [12] and protection against corrosion [13], or embedded in multilayer systems as in devices for control of terahertz waves [14] and touch-panel

displays [15]. In many cases a strong interaction with the substrate is required, at least at specific locations, as to securely clamp the edge of a freestanding nanoscale resonator [16] or the boundary of a membrane for mechanical tests [17], [18], [19], [20], [21] or to induce strain through a flexible substrate in order to investigate strain engineering properties [22]; whereas in many others the interaction should be as low as possible, as in electro-mechanical switches, or of medium intensity, in order to have well-adhered but sliding graphene flakes able to fold in nanoribbons [23].

Thus, a deep understanding of the mechanism behind the interaction of graphene with a substrate is not only interesting from a fundamental point of view but becomes necessary when applications in electronics are considered. Unfortunately, the origin of such interaction still remains an open question and a satisfactory explanation still lacks [24] in spite of a number of both numerical [25], [10], [26] and experimental [27] [28], [29], [30] studies.

The investigated substrate materials span over metals, like Ni and Cu [29], to silicon oxide, a common insulator in electronic devices. The first measurement of the adhesion energy of a monolayer graphene on SiO₂ revealed a surprisingly high interaction, which was ascribed to the graphene ability to conform in a liquid-like fashion over even smooth surfaces [28]. According to a common understanding, the interaction of graphene with SiO₂ is believed to be controlled by weak, long-range van der Waals forces emerging between instantaneous/induced dipoles forming in either graphene or SiO₂ [31], [32]. A similar mechanism is known to determine also the adhesion of micromachined surfaces [33]. However, it was recently demonstrated by multiscale modeling [31] that van der Waals forces alone cannot explain the high tensile and shear toughness of graphene/SiO₂ interface as found in adhesion experiments. As an alternative explanation, was adduced the possible role played by surface defects, such as undercoordinated Si atoms and non-bridging O atoms, to which graphene can bind. As a matter of fact, no sufficient attention has ever been paid to the presence of charges either within the oxide layer or located at its surface that can strongly interact with graphene. Nevertheless, it is well known in microelectronics that the growth of oxide on top of Si wafers causes residual charges to develop at the interface [34]. In addition,

SiO₂ surface is known to be rich of silanol groups (Si-OH). These originate from the interaction of silica with water molecules in air and commonly undergo protonation reactions [35], which leave significant surface charges.

Thus, in the present work we explore how such charge sources can be responsible for the strong interaction of graphene with SiO₂-based substrates.

2. Experimental

2.1 Graphene preparation. Monolayer Graphene samples were grown using a copper (Cu) foil catalyst by Chemical Vapor Deposition (CVD). Graphene synthesis was carried out in a cold walled CVD reactor (Aixtron BM) at 1000 °C and at low pressure using methane as the carbon source. Prior to the growth the Cu foils were chemically treated in order to clean and smoothen the surface followed by annealing at 1000 °C under hydrogen and argon flow. After the synthesis, a poly(methyl methacrylate) (PMMA) sacrificial support layer was spin coated onto the graphene covered Cu foil. Cu was chemically etched using a ferric chloride containing solution followed by different cleaning steps in distilled water and acid solutions. The monolayer graphene was transferred onto different substrates. The film was dried at 120°C for few hours and finally, the PMMA layer was removed by dipping into acetone and IPA.

2.2 Raman spectroscopy. Raman measurements were carried out on a LabRAM Aramis (HORIBA Jobin Yvon, France, with a 632.8 nm laser at a magnification of 50x and grating width of 1200. Spectra were acquired with an integration time of 5s repeated twenty times. The data reported refer to the mean of 6 measurements at different locations on the same sample. Before the analysis, all the samples were cleaned by thermal annealing at 500°C for 1h with the only exception of Si covered with CH₄+H₂, which would receive severe damage from the high temperature treatment.

2.3 Amplitude Modulation-Scanning Kelvin Probe Microscopy. The images were acquired with an Atomic Force Microscope (AFM) named Solver Px by NT-MDT. AFM topographical data were acquired in semi-contact mode while surface potential was measured using the Amplitude Modulation-Scanning Kelvin Probe Microscopy (SKPM). SKPM is a two-pass technique. After the topographical scan (which resulted to be the same in both trace and retrace) the tip is lifted up 10 nm off the sample surface and the surface potential data are acquired at a fixed distance from the sample surface. We used noncontact high resolution silicon cantilevers NSG10 series with PtIr conductive coating. The thickness of the coating is 20-30nm and the typical tip curvature radius is 35nm. Tips were electrically calibrated against fresh exfoliated graphite. The results reported in the manuscript are obtained from repeated analyses made on different samples whose number depends on the signal variability. For TO, the data refers to the average of 9 mean CPD values- each referring to a random region of few tens μm^2 area- made in different days. For TO+AN and NO samples the data refers to an average of 5 mean CPD values- each referring to a random region of few tens μm^2 area- made in different days. For TEOS and TEOS+AN samples the data refers to an average of 4 and 5, respectively, mean CPD values- each referring to a random region of few tens μm^2 area- made in different days. For the Si+CH₄+H₂ sample the variability was very low and data refers to an average of 2 mean CPD values- each referring to a random region of few tens μm^2 area- made on the same day. Different quartz samples were measured in different days but the variability was always too large to provide enough statistical significance.

2.4 XPS analysis. The Axis Ultra XPS spectrometer by Kratos UK, was calibrated with respect to the Au 4f 7/2 peak position fixed at 84.00 eV for a polycrystalline Au foil. The Fermi-level position was then obtained considering the inflection point of the signal intensity on the Au Fermi Edge following the procedure of the instrument manufacturer. Spectra were acquired using a pass energy of 80 eV and an energy step of 0.1eV. 20 sweeps were acquired for each of the VB spectra to obtain a good signal-to-noise ratio.

3. Results and discussion

In order to highlight the role of surface charges of SiO₂ in its interaction with graphene, we considered a number of Si/SiO₂ substrates with different amount of superficial charge. These substrates were fabricated by varying three main parameters, namely, the silicon crystal orientation (a), the oxide growth process (b) and the thermal treatment after the oxide formation (c). With reference to the first parameter (a), rectangular slices were cut from either a 111 Si wafer or non-crystalline Quartz wafer. Then, (b) three types of oxide were considered. The first is the native oxide (NO), which naturally grows from the exposure of a Si wafer to air. The other two oxides (300 nm thick in both cases) were obtained by either thermal growth through direct oxidation of a 111 Si wafer (thermal oxide, TO) or deposition from a tetraethylorthosilicate precursor (TEOS). (c) After oxide deposition/growth, some samples were annealed at 950°C for 30 minutes in N₂ atmosphere (see SI for more details about sample preparation). The last type of sample was derived from a 111 Si wafer where a thin layer (in the range of 5-10 nm) of CH₄+H₂ was deposited after HF etching the native oxide. The variation of the previous three process parameters implied the availability of 7 different substrates, and on each of them a monolayer graphene produced by Chemical Vapor Deposition (CVD) was transferred following a standard protocol (details in the Methods section).

In order to characterize the interaction of graphene with each substrate, Raman spectroscopy was employed. Although Raman spectroscopy is generally used to assess the quality of graphene based films, it can also be effectively employed for the evaluation of substrate/graphene interactions [36]. Indeed, as it probes the vibrational states of a system of atoms, Raman spectroscopy is sensitive to an even minimum modification of their electronic structure [37], [38], including the doping level [39] and the interaction with exogeneous chemical species. For example, it has been demonstrated that oxygen molecules adsorbed on SiO₂ are able to interact with the aromatic rings of graphene thus modifying its charge distribution [40], [41], [42], [43].

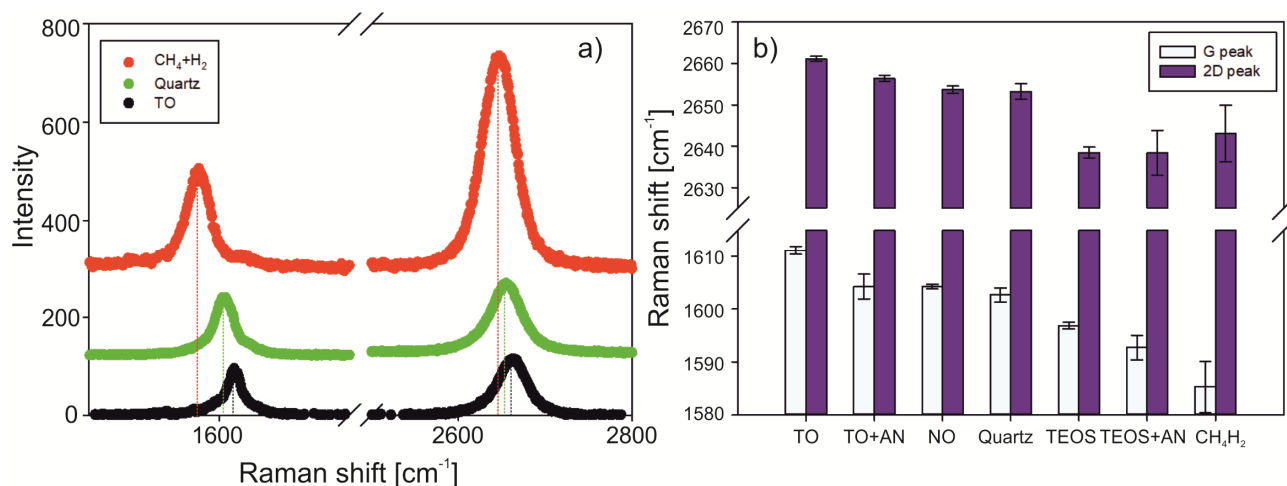


Figure 1: a) Raman spectra of graphene transferred on a 111 Si wafer with thermal oxide on top (TO), Quartz and 111 Si with a thin layer of CH₄+H₂ (aC:H) deposited on top after etching its native oxide. A blue-shift of both G and 2D peaks is visible when graphene is on either Quartz or TO with respect to graphene on Si111 with CH₄+H₂ layer. b) Position of the G and 2D peaks of Raman spectra recorded for graphene on different Silicon-based substrates: Quartz, Si 111 with annealed thermal oxide (TO), 111 Si with thermal oxide on top, Si 111 with native oxide, Si 111 with TEOS oxide, Si 111 with annealed TEOS, 111 Si with a thin layer of CH₄+H₂ deposited after etching of Si native oxide with HF.

The vibrational mode characteristics (eg peak position and bandwidth) are also sensitive to the application of stress or strain from the environment or substrate. This suggests that in our case the effect of a different preparation of our SiO₂ surfaces should induce detectable changes in the Raman spectra of graphene depending on the strength of its interaction with the substrate [44], [45]. Similar indications are given by both theoretical [10], [46] and experimental works [47] [36]. Indeed, the Raman spectra of our samples differ from one another in many respects, such as the position and broadening of the graphene characteristic G and 2D peaks, as well as their relative intensity (Figures 1a, S1 and Table S1). Let us first consider the positions of the G and 2D peaks (Figure 1b).

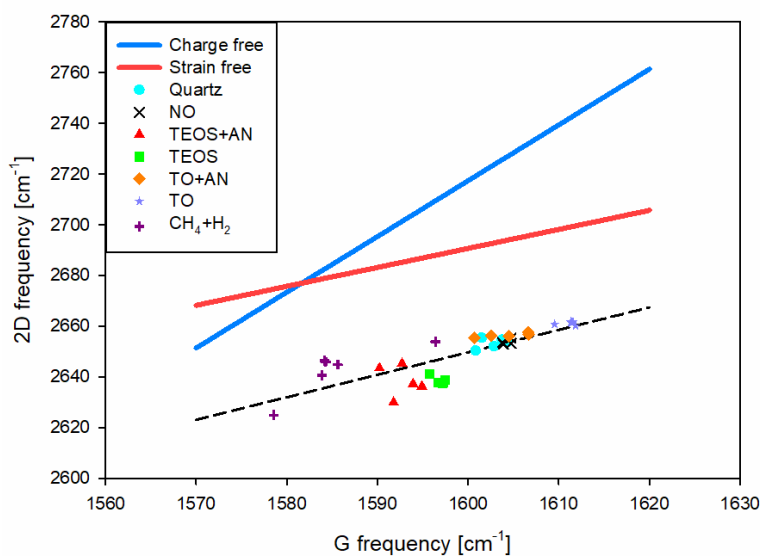


Figure 2: Frequency of the 2D peak vs the frequency of the G peak of a monolayer graphene deposited on different silicon substrates. The experimental points can be fitted by a line (dashed in the plot) that results to be parallel to the reference line corresponding to a graphene sample with no strain (strain free line in red).

As stated before, a shift of the Raman peaks can be related to different factors, mainly including the doping and the strain that can be induced, even uncontrollably, during the fabrication process. In fact, even if the samples are prepared according to the same protocol, as in our case, still differences may arise. In order to deconvolute the mechanical contribution to the Raman shift from that due to the electrical charges in graphene, it is useful to study the relative position of the G and 2D peaks across our samples. According to a previously reported methodology [48], in the G frequency-2D frequency plane, it is possible to identify two reference lines that represent graphene samples showing either no doping or no strain (blue and red lines in Figure 2, respectively). The intersection of these two lines defines a reference point O with coordinates $(1581.6; 2676.9) \text{ cm}^{-1}$ corresponding to a sample with zero strain and zero charge. Interestingly, if we plot the Raman 2D frequencies against the G frequencies of all our samples, we can draw about 40 data points that result to be well aligned. Considering a regression fit, the slope of the fitting line is 0.89 that is much smaller than the charge free line, whose slope is reported as 2.02–2.44 [48], yet it matches very well the slope of the free strain line that is reported to be 0.75 ± 0.04 [48]. From this evidence, we can reasonably

state that no significant difference in strain can be observed across our samples. This same conclusion emerges if we compute and compare the strain of each sample as follows. For each point representing our samples we can draw a line - parallel to the free strain line - whose intersection with the free charge line defines a new point with an associated G frequency. Its frequency shift, $\Delta\omega_G$, from the reference point O allows to estimate the corresponding hydrostatic strain, ε_h , as [49]:

$$\varepsilon_h = -\Delta\omega_G / \omega_0 \gamma \quad (1)$$

where ω_0 is the G frequency of the reference point O and γ is the Grüneisen parameter equal to 1.8 [49] (more details can be found in the SI). Overall, the mean hydrostatic strain, $\varepsilon_h = \varepsilon_{xx} + \varepsilon_{yy}$, across all the samples is $1.0\% \pm 0.1\%$. If we assumed a biaxial strain, ε_b , on our graphene samples, this would be half of the computed hydrostatic strain, i.e. $\varepsilon_b = \varepsilon_{xx} = \varepsilon_{yy} = 0.5\%$. Such value matches very well the strain due to friction of water when a graphene sheet is deposited through wet transfer on a Si substrate (more details in the SI).

Then, since no significant difference in strain can be observed, we can argue that the main factor causing the shift of the Raman peaks from one sample to the other is the presence of charges in graphene. Furthermore, from the same 2D-G frequencies plot and following the same approach previously considered in the case of the strain, we can derive the amount of charge affecting each sample, too. In particular, since the sensitivity of the 2D peak frequency against the number of charges for unit area is about $0.7 \cdot 10^{-12}$ ($1 \cdot 10^{-12}$) cm^2/cm [35], [51], from the projection of the border points along the free strain axis, we can find that the amount of charge across our samples vary between 3.2 (2.2) $\cdot 10^{13} \text{ cm}^{-2}$ (graphene on Si with a CH_4+H_2 layer) and 6.0 (4.2) $\cdot 10^{13} \text{ cm}^{-2}$ (graphene on Si with TO on top). More details about such estimation are reported in the SI.

Overall, a difference of about 2.7 (1.9) $\cdot 10^{13} \text{ cm}^{-2}$ charge density across our samples causes a blue shift of the G frequency of up to 26 cm^{-1} that is then comparable with the concentration of electrons/holes able to cause a 21 (17) cm^{-1} blue shift of the Raman G peak as previously reported [38].

Both the values of strain and doping that we derived depend on the slope of the zero charge and zero strain lines. However, while in the case of the zero-charge line there is a good agreement in the literature, more uncertainties still affect the estimation of the zero strain line with reported values ranging between $0.55 \pm 0.2 - 0.75 \pm 0.05$ [52] [48] [38].

It is now interesting to explore the origin of the different doping level across our graphene samples. It was recently reported that in the case of a strong interaction with an external charge (distribution), as in our case [53], [54] graphene behaves like a metal where the external charge distribution induces the development of image charges [54]. As a consequence, we can argue that since our graphene samples are always deposited onto polar SiO₂ surfaces, they develop an image charge that matches in magnitude that of the underlying SiO₂ [54]. Thus, differences in the graphene charge, as revealed by the analysis of Raman spectra, are to be ascribed to variations in the charges amount of our SiO₂ substrates. The sample showing the highest blue shift (e.g., highest charge amount) corresponds to graphene deposited on Si with thermal oxide (TO) on top, whereas the sample with the lowest blue shift corresponds to Si with a CH₄+H₂ layer. In between, there are those with either TEOS oxides (TEOS and TEOS+AN). The observed differences can be explained considering the process used to fabricate the Si oxide layer. In the case of TO type, the growth of the thermal oxide proceeds at the expense of the underlying Si wafer, thus inducing a distortion of the Si crystal lattice at the interface. Such a distortion is accompanied by the formation of a residual electrical charge (that can be estimated as $<10^{12} \text{ cm}^{-2}$ [55]). However, this residual charge is much more limited than that of TEOS, where the quality of the oxide is lower and characterized by the presence of a charge density of $\sim 10^{12} \text{ cm}^{-2}$. A method commonly used in electronics to reduce such a charge density is annealing at high temperatures (950 °C) which induces a relaxation of the inner strains and a reduction of the charge to $\sim 10^{10} \text{ cm}^{-2}$. Thus, in the hypothesis of electrostatic interaction between graphene and the substrate, we expect that a thermal process would reduce the intensity of their interaction. Indeed, this explains why the blue shift of G (2D) peak for a given substrate is lower when thermal annealing is introduced. Furthermore, as a limiting case, the absence of the oxide

layer (e.g., the native oxide is etched and the underlying substrate is covered with a CH₄+H₂ layer) should provide the smallest amount of residual charge, that in turn should provide the lowest graphene interaction. As a confirmation, the CH₄+H₂ substrate provides the most red-shifted G peak in the Raman spectra. However, if we consider only the amount of charge embedded in the oxide layer, we could not explain why TO substrates provide more interaction than TEOS substrates (Figure 1b). Indeed, apart from the charge embedded in the oxide, it is well known that SiO₂ interacts with water (even in ambient conditions) with the formation of silanol groups on its surface. Such groups are then subjected to protonation reactions [35] that cause the formation of an even significant amount of surface charge (up to 10¹⁴ cm⁻²), which is much higher than the residual interface charge [55], [56]. Overall, the amount of surface charge expected on SiO₂ as a consequence of both the fabrication process and protonation reactions is compatible with the estimation derived from the analysis of the Raman spectra. Other evidences of the presence of charges in graphene come from an analysis of the FWHM of the G peak. In a previous study [38] it was shown that the FWHM significantly decreases when the number of charges in graphene increases up to 5 · 10¹² cm⁻². Then, it stabilizes within the range 6 cm⁻¹ – 11 cm⁻¹. Interestingly, this is the same interval that includes the G peak FWHM of all our samples (Table S1), which thus results to be compatible with the presence of few 10¹³ cm⁻² charges as we identified from the G (2D) frequency shift. Similarly, the relative intensity of the 2D and G peak, I_{2D}/I_G, decreases significantly when the number of charges in graphene increases up to 5 · 10¹² cm⁻². Then, the reduction trend is much less pronounced and for a number of charge bigger than 5 · 10¹² cm⁻², I_{2D}/I_G was reported to be smaller than 1.5 [38], which matches our experimental evidence (Table S1). The only I_{2D}/I_G slightly bigger in our experiments (1.65 ± 0.76) was recorded for the CH₄+H₂ sample, which has the smallest amount of electrical charge, though.

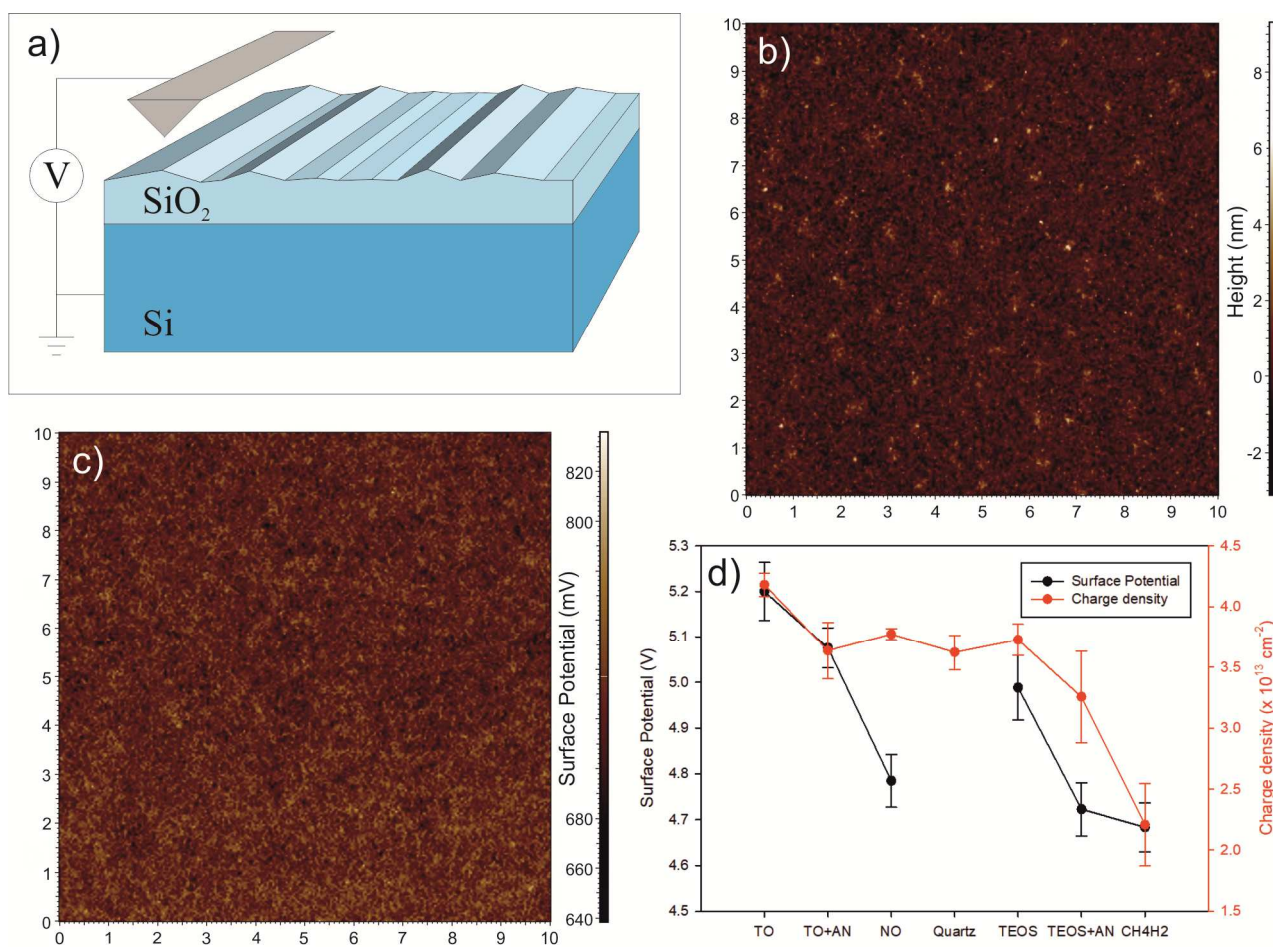


Figure 3: a) Surface potential measurement setup. During the measurement, each Si/SiO₂ substrate is grounded. b) Example topographical and (c) surface potential maps derived from the KPFM tip scanning a 10 x 10 μm^2 sample surface area. Before the electrical measurement, the SKPM tip was calibrated against a reference graphite sample; d) Comparison of the surface potential measured for different Si substrates (Si 111 with thermal oxide (TO) treated with thermal annealing (AN), quartz, Si 111 with thermal oxide on top, Si 111 with TEOS oxide, Si 111 with TEOS oxide treated with thermal annealing (AN), Si 111 with a thin layer of CH₄H₂ deposited after etching its native oxide with HF, Si 111 with native oxide) and expressed as absolute difference with respect to graphite work function. The surface potential data are compared to the Raman G frequency recorded for a graphene sheet deposited on each of the considered substrates.

In order to confirm that the strong interaction of graphene and SiO₂ is related to the amount of surface charges of our Si/SiO₂ substrates, we measured the surface potential of these latter through Amplitude Modulated-Scanning Kelvin Probe Microscopy (AM-SKPM). AM-SKPM is a non-contact method for direct measurement of the contact potential difference between an Atomic Force Microscope (AFM) tip and a sample surface [57] (Figure 3a). Since the contact potential difference (CPD) between two materials depends on a variety of parameters, such as the work function [58] and dopant concentration in semiconductors [59], this can provide information about the whole

surface charge, including both the contributions of the embedded charge and the charge due to polar groups on the substrate surface [60]. For the quantitative measurement of CPD distribution, before the experiments, the tip of the SKPM was first calibrated against fresh exfoliated graphite (HOPG) and then used to scan each substrate in order to have a map of its topography and surface potential (Figure 3b-c). The surface potential of each substrate, V_s , was evaluated according to the following equation:

$$V_s = CPD + V_T \quad (2)$$

where CPD is measured directly by the instrument and V_T is the tip surface potential. This latter can be computed as $V_{HOPG} - CPD_{cal}$, where CPD_{cal} is the contact potential distribution measured by the instrument during the tip calibration and V_{HOPG} is the HOPG surface potential, assumed here equal to 4.475 V [61].

Figure 3d reports the surface potential of each substrate directly measured by SKPM as compared to the charge density of the corresponding graphene sample on top derived from the interpretation of the Raman spectra according to the previously discussed procedure. Surprisingly, the variations of the surface potential and graphene charge density across the different substrates are in general agreement with one another despite they refer to different physical entities measured through different techniques. Some differences can be noted only in the case of NO and CH₄+H₂ and these can be explained by the same reason, though. Indeed, both the samples consist of a few nanometers thick layer laying on a bulk silicon substrate. From the literature it is well known that SKPM can reach a depth sensitivity of several hundreds of nanometers, which enables it to detect objects located beneath the scanned surface [62]. Thus, it is very likely that the CPD measured in our SKPM tests takes into account not only the surface potential strictly related to the thin film of interest, but also the substrate contribution. In addition, this contribution affects differently NO and CH₄+H₂. In the first case, since Si has higher conductivity than NO, we expect that the substrate presence causes a reduction of the measured surface potential (i.e., the corresponding value reported in Figure 3d is underestimated). On the contrary, in the second case, as the CH₄+H₂ film is more

conductive than Si, we expect an overestimation of the measured CPD (i.e., the actual value is smaller than the reported one). The relatively high depth sensitivity of SKPM explains also the unavailability of stable data for quartz, which is not reported in Figure 3d, with respect the other substrates. In fact, the experimental condition for the SKPM measurement on quartz involves testing of a 600 μm thick bulk sample, whereas in all the other cases, the tested samples consist of oxide layers of at least 300nm thickness laying on a bulk Si substrate connected to the ground. Since the SKPM tip has a relatively high depth sensitivity, the presence of the Si bulk played a beneficial role in stabilizing the measurement on the upmost oxide layer. On the contrary, in the case of quartz, the surface to be tested belongs to a bulk dielectric material, which is not possible to ground. This causes the electrical measurement to be unstable and thus not reliable.

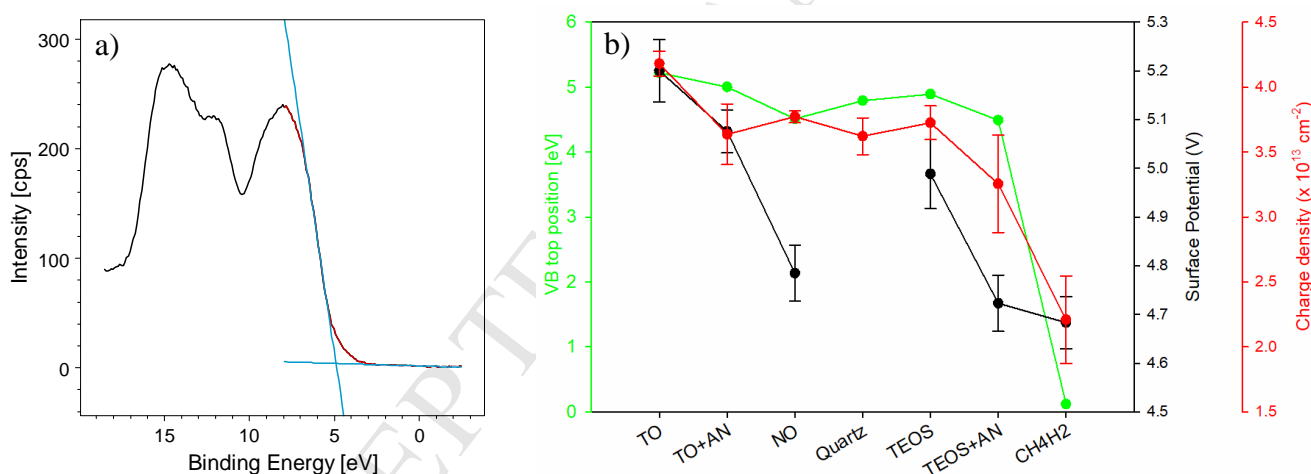


Figure 4: a) Valence Band (VB) of a TEOS sample derived from XPS measurement. According to a conventional linear fit algorithm, the top of the VB is determined as the intersection between the linear fit of the falling shoulder of the VB and the VB background above the Fermi level; b) Position of the Valence band Top estimated for different Si based substrates: 111 Si with thermal oxide on top, 111 Si with thermal oxide on top and treated with thermal annealing, 111 Si with native oxide, quartz, Si 111 with TEOS oxide, 111 Si with TEOS oxide and treated with thermal annealing, Si 111 with a thin layer of CH_4+H_2 deposited after etching its native oxide with HF.

Finally, in order to have the ultimate evidence that there is a difference in the amount of surface dipoles across our substrates, we performed X-ray Photoelectron Spectroscopy (XPS) analysis. This

allows for an estimation of the Valence Band (VB) top position, which is in turn sensitive to the surface charge distribution caused by dipoles.

In oxidized silicon samples, a negative surface charge is expected due to the charge transfer from silicon to oxygen in positively doped samples as ours. Negative charges induce a downward band bending that increases the distance between the VB-top and the Fermi level [63], [64]. The opposite occurs when positive charges accumulate on the sample surface that lead instead to an upward band bending. Since in our analysis, the Fermi level was carefully aligned to zero utilizing a polycrystalline sputtered gold sample, the differences in the VB-top result from the different surface composition. In particular, the higher the band bending the more negative the surface charge. Alternatively, we can say that the higher the potential measured by the SKPM, the higher the regression of the VB-top from the Fermi level due to band bending.

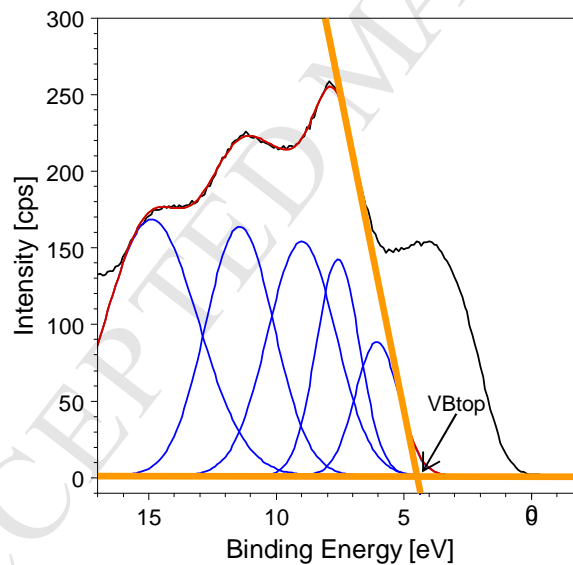


Figure 5: Valence band (VB) of an example 111 Si sample with a native oxide layer on top and evaluation of the VB-top after eliminating the contribution of bulk Si.

Indeed, we find a good agreement between the trend of the band bending induced by the charge accumulation on the sample surface with the surface potential measured by SKPM (Figure 4b) and the graphene charge density previously estimated through Raman spectroscopy. In this regard, the only slight outlier is the NO sample. However, in this latter case the estimation of VB-top position

was more complex as a consequences of additional features of NO valence band with respect to the other samples (see Figures 4a and 5). Indeed, we observed a shoulder near the Fermi edge which can be assigned to a non-negligible density of states near the Fermi edge due to the semiconducting nature of the underlying bulk Si substrate, as already described in the literature by experimental and theoretical works [65] [66] [67] [68]. Differently from the other samples, in this case we are sensitive to the bulk Si because the native oxide layer is very thin and in particular it is thinner than the sampling depth of the X-rays for photoelectrons at ~ 1480 eV.

To estimate the position of the VB top in the case of the NO sample, the contribution of the silicon substrate was firstly eliminated through a Gaussian fitting procedure (see SI) and then the top of the valence band was evaluated through a linear fit as for the other samples (Figure 5). Our estimation of 4.51eV results in very good agreement with data reported in literature [66], but an underestimation with respect to the other samples cannot be excluded because of the additional analysis required.

4. Conclusions

In this work the interaction between graphene and SiO₂ was proven to be related to the electrical charges at the SiO₂ surface originating from both the oxide fabrication process and protonation reactions. This clue results from experimental evidences obtained through different and independent physical techniques including Raman spectroscopy, Scanning Kelvin Probe Microscopy and X-ray Photoelectron Spectroscopy.

Raman analyses performed on graphene monolayers deposited onto different oxidized Si substrates obtained by induced oxidation or by deposition of silica from TEOS, revealed that each sample interacts with its substrate through an electrostatic interaction which depends on the amount of surface charges. The presence of a varying surface charge across our substrates was also confirmed by both SKPM, through a direct measurement of their surface potential, and XPS analyses, through an estimation of their valence band bending. Interestingly, the SiO₂/Si substrates characterized by

higher/lower charge correspond to higher/lower interaction with graphene. Our results indicate that substrate surface charges, if properly controlled, may enable tuning the graphene and 2D materials interaction with different substrates. Such mechanism can open new frontiers in microelectronics and can then be exploited in novel multifunctional devices providing strong adhesion only at particular locations and for even large areas.

Acknowledgements

The authors wish to thank Dr. Konstantinos Papagelis and Nick Delikoukos for deposition of graphene on NO and quartz substrates.

NMP and CG are supported by the European Commission H2020 under the Graphene Flagship Core 2 No. 785219 (WP14 “Composites”). NMP is also supported by the European Commission H2020 under the FET Proactive “Neurofibres” Grant No. 732344 as well as by the Italian Ministry of Education, University and Research (MIUR) under the “Departments of Excellence” grant L.232/2016.

AC and AZ are supported by European Commission under the Graphene Flagship (WP15 “Production”).

References

- [1] A.C. Ferrari, F. Bonaccorso, V. Fal’ko, K.S. Novoselov, S. Roche, P. Boggild, S. Borini, F.H.L. Koppens, V. Palermo, N. Pugno, J.A. Garrido, R. Sordan, A. Bianco, L. Ballerini, M. Prato, E. Lidorikis, J. Kivioja, C. Marinelli, T. Ryhanen, A. Morpurgo, J.N. Coleman, V. Nicolosi, L. Colombo, A. Fert, M. Garcia-Hernandez, A. Bachtold, G.F. Schneider, F. Guinea, C. Dekker, M. Barbone, Z. Sun, C. Galiotis, A.N. Grigorenko, G. Konstantatos, A. Kis, M. Katsnelson, L. Vandersypen, A. Loiseau, V. Morandi, D. Neumaier, E. Treossi, V. Pellegrini, M. Polini, A. Tredicucci, G.M. Williams, B. Hee Hong, J.-H. Ahn, J. Min Kim, H. Zirath, B.J. van Wees, H. van der Zant, L. Occhipinti, A. Di Matteo, I.A. Kinloch, T. Seyller, E. Quesnel, X. Feng, K. Teo, N. Rupesinghe, P. Hakonen, S.R.T. Neil, Q. Tannock, T. Lofwander, J. Kinaret, Science and technology roadmap for graphene, related two-dimensional crystals, and hybrid systems, *Nanoscale*. 7 (2015) 4598–4810. doi:10.1039/C4NR01600A.
- [2] A.K. Geim A.K., Novoselov K.S., The rise of graphene, *Nat. Mater.* 6 (2007) 183–191.
- [3] D. Jariwala, T.J. Marks, M.C. Hersam, Mixed-dimensional van der Waals heterostructures, *Nat. Mater.* 16 (2016) 170–181. doi:10.1038/nmat4703.

- [4] R. Dong, L. Moore, L.E. Ocola, I. Kuljanishvili, Enabling Quality Interfaces with Mask-Free Approach to Selective Growth of MoS₂/Graphene Stacked Structures, *Adv Mater Interfaces*. 3 (2016) 1600098.
- [5] T.O. Wehling, K.S. Novoselov, S.V. Morozov, E.E. Vdovin, M.I. Katsnelson, A.K. Geim, A.I. Lichtenstein, Molecular Doping of Graphene, *Nano Lett.* 8 (2008) 173–177. doi:10.1021/nl072364w.
- [6] X. Fan, L. Liu, J.-L. Kuo, Z. Shen, Functionalizing Single- and Multi-layer Graphene with Br and Br₂, *J. Phys. Chem. C*. 114 (2010) 14939–14945. doi:10.1021/jp1041537.
- [7] D.C. Elias, R.R. Nair, T.M.G. Mohiuddin, S.V. Morozov, P. Blake, M.P. Halsall, A.C. Ferrari, D.W. Boukhvalov, M.I. Katsnelson, A.K. Geim, K.S. Novoselov, Control of Graphene's Properties by Reversible Hydrogenation: Evidence for Graphane, *Science*. 323 (2009) 610–613. doi:10.1126/science.1167130.
- [8] J.-H. Kim, J.H. Hwang, J. Suh, S. Tongay, S. Kwon, C.C. Hwang, J. Wu, J. Young Park, Work function engineering of single layer graphene by irradiation-induced defects, *Appl. Phys. Lett.* 103 (2013) 171604. doi:10.1063/1.4826642.
- [9] Y.-J. Kang, J. Kang, K.J. Chang, Electronic structure of graphene and doping effect on SiO₂, *Phys. Rev. B*. 78 (2008). doi:10.1103/PhysRevB.78.115404.
- [10] X.F. Fan, W.T. Zheng, V. Chihaiia, Z.X. Shen, J.-L. Kuo, Interaction between graphene and the surface of SiO₂, *J. Phys. Condens. Matter*. 24 (2012) 305004. doi:10.1088/0953-8984/24/30/305004.
- [11] J. Bai, X. Zhong, S. Jiang, Y. Huang, X. Duan, Graphene nanomesh, *Nat. Nanotechnol.* 5 (2010) 190–194. doi:10.1038/nnano.2010.8.
- [12] K.-S. Kim, H.-J. Lee, C. Lee, S.-K. Lee, H. Jang, J.-H. Ahn, J.-H. Kim, H.-J. Lee, Chemical Vapor Deposition-Grown Graphene: The Thinnest Solid Lubricant, *ACS Nano*. 5 (2011) 5107–5114. doi:10.1021/nn2011865.
- [13] D. Prasai, J.C. Tuberquia, R.R. Harl, G.K. Jennings, K.I. Bolotin, Graphene: Corrosion-Inhibiting Coating, *ACS Nano*. 6 (2012) 1102–1108. doi:10.1021/nn203507y.
- [14] S.H. Lee, M. Choi, T.-T. Kim, S. Lee, M. Liu, X. Yin, H.K. Choi, S.S. Lee, C.-G. Choi, S.-Y. Choi, X. Zhang, B. Min, Switching terahertz waves with gate-controlled active graphene metamaterials, *Nat. Mater.* 11 (2012) 936–941. doi:10.1038/nmat3433.
- [15] G. Anagnostopoulos, P.-N. Pappas, Z. Li, I.A. Kinloch, R.J. Young, K.S. Novoselov, C.Y. Lu, N. Pugno, J. Parthenios, C. Galiotis, K. Papagelis, Mechanical Stability of Flexible Graphene-Based Displays, *ACS Appl. Mater. Interfaces*. 8 (2016) 22605–22614. doi:10.1021/acsami.6b05227.
- [16] J.S. Bunch, A.M. van der Zande, S.S. Verbridge, I.W. Frank, D.M. Tanenbaum, J.M. Parpia, H.G. Craighead, P.L. McEuen, Electromechanical Resonators from Graphene Sheets, *Science*. 315 (2007) 490–493. doi:10.1126/science.1136836.
- [17] J.S. Bunch, S.S. Verbridge, J.S. Alden, A.M. van der Zande, J.M. Parpia, H.G. Craighead, P.L. McEuen, Impermeable Atomic Membranes from Graphene Sheets, *Nano Lett.* 8 (2008) 2458–2462. doi:10.1021/nl801457b.
- [18] C. Lee, X. Wei, J.W. Kysar, J. Hone, Measurement of the Elastic Properties and Intrinsic Strength of Monolayer Graphene, *Science*. 321 (2008) 385–388. doi:10.1126/science.1157996.
- [19] G.-H. Lee, R.C. Cooper, S.J. An, S. Lee, A. van der Zande, N. Petrone, A.G. Hammerberg, C. Lee, B. Crawford, W. Oliver, J.W. Kysar, J. Hone, High-Strength Chemical-Vapor-Deposited Graphene and Grain Boundaries, *Science*. 340 (2013) 1073–1076. doi:10.1126/science.1235126.
- [20] J.-U. Lee, D. Yoon, H. Cheong, Estimation of Young's Modulus of Graphene by Raman Spectroscopy, *Nano Lett.* 12 (2012) 4444–4448. doi:10.1021/nl301073q.
- [21] M.F. Pantano, G. Speranza, C. Galiotis, N. Pugno, A mechanical system for tensile testing of supported films at the nanoscale, *Nanotechnology*. 29 (2018) 395707. doi:10.1088/1361-6528/aacf50.

- [22] S. Deng, A.V. Sumant, V. Berry, Strain engineering in two-dimensional nanomaterials beyond graphene, *Nano Today*. 22 (2018) 14–35. doi:10.1016/j.nantod.2018.07.001.
- [23] J. Annett, G.L.W. Cross, Self-assembly of graphene ribbons by spontaneous self-tearing and peeling from a substrate, *Nature*. 535 (2016) 271–275. doi:10.1038/nature18304.
- [24] J.S. Bunch, M.L. Dunn, Adhesion mechanics of graphene membranes, *Solid State Commun.* 152 (2012) 1359–1364. doi:10.1016/j.ssc.2012.04.029.
- [25] Y. He, W.F. Chen, W.B. Yu, G. Ouyang, G.W. Yang, Anomalous interface adhesion of graphene membranes, *Sci. Rep.* 3 (2013). doi:10.1038/srep02660.
- [26] W. Gao, P. Xiao, G. Henkelman, K.M. Liechti, R. Huang, Interfacial adhesion between graphene and silicon dioxide by density functional theory with van der Waals corrections, *J. Phys. Appl. Phys.* 47 (2014) 255301. doi:10.1088/0022-3727/47/25/255301.
- [27] P. Gong, Q. Li, X.Z. Liu, R.W. Carpick, P. Egberts, Adhesion mechanics between nanoscale silicon oxide tips and few-layer graphene, *Tribol Lett.* 65 (2017) 61–75.
- [28] S.P. Koenig, N.G. Boddeti, M.L. Dunn, J.S. Bunch, Ultrastrong adhesion of graphene membranes, *Nat. Nanotechnol.* 6 (2011) 543–546. doi:10.1038/nnano.2011.123.
- [29] S. Das, D. Lahiri, D.-Y. Lee, A. Agarwal, W. Choi, Measurements of the adhesion energy of graphene to metallic substrates, *Carbon*. 59 (2013) 121–129. doi:10.1016/j.carbon.2013.02.063.
- [30] Z. Zong, C.-L. Chen, M.R. Dokmeci, K. Wan, Direct measurement of graphene adhesion on silicon surface by intercalation of nanoparticles, *J. Appl. Phys.* 107 (2010) 026104. doi:10.1063/1.3294960.
- [31] S. Kumar, D. Parks, K. Kamrin, Mechanistic Origin of the Ultrastrong Adhesion between Graphene and α -SiO₂: Beyond van der Waals, *ACS Nano*. 10 (2016) 6552–6562. doi:10.1021/acsnano.6b00382.
- [32] M. Ishigami, J.H. Chen, W.G. Cullen, M.S. Fuhrer, E.D. Williams, Atomic Structure of Graphene on SiO₂, *Nano Lett.* 7 (2007) 1643–1648. doi:10.1021/nl070613a.
- [33] F.W. DelRio, M.P. de Boer, J.A. Knapp, E. David Reedy, P.J. Clews, M.L. Dunn, The role of van der Waals forces in adhesion of micromachined surfaces, *Nat. Mater.* 4 (2005) 629–634. doi:10.1038/nmat1431.
- [34] B.E. Deal, M. Sklar, A.S. Grove, E.H. Snow, Characteristics of the surface-state charge (Q_{ss}) of thermally oxidized silicon, *J. Electrochem. Soc.* 114 (1967) 266–274. <http://jes.ecsdl.org/content/114/3/266.short> (accessed June 21, 2017).
- [35] B.M. Lowe, C.-K. Skylaris, N.G. Green, Acid-base dissociation mechanisms and energetics at the silica-water interface: An activationless process, *J. Colloid Interface Sci.* 451 (2015) 231–244. doi:10.1016/j.jcis.2015.01.094.
- [36] S.M. Song, B.J. Cho, Investigation of interaction between graphene and dielectrics, *Nanotechnology*. 21 (2010) 335706. doi:10.1088/0957-4484/21/33/335706.
- [37] C. Casiraghi, S. Pisana, K.S. Novoselov, A.K. Geim, A.C. Ferrari, Raman fingerprint of charged impurities in graphene, *Appl. Phys. Lett.* 91 (2007) 233108. doi:10.1063/1.2818692.
- [38] A. Das, S. Pisana, B. Chakraborty, S. Piscanec, S.K. Saha, U.V. Waghmare, K.S. Novoselov, H.R. Krishnamurthy, A.K. Geim, A.C. Ferrari, A.K. Sood, Monitoring dopants by Raman scattering in an electrochemically top-gated graphene transistor, *Nat. Nanotechnol.* 3 (2008) 210–215. doi:10.1038/nnano.2008.67.
- [39] M. Kalbac, A. Reina-Cecco, H. Farhat, J. Kong, L. Kavan, M.S. Dresselhaus, The Influence of Strong Electron and Hole Doping on the Raman Intensity of Chemical Vapor-Deposition Graphene, *ACS Nano*. 4 (2010) 6055–6063. doi:10.1021/nn1010914.
- [40] S. Ryu, L. Liu, S. Berciaud, Y.-J. Yu, H. Liu, P. Kim, G.W. Flynn, L.E. Brus, Atmospheric Oxygen Binding and Hole Doping in Deformed Graphene on a SiO₂ Substrate, *Nano Lett.* 10 (2010) 4944–4951. doi:10.1021/nl1029607.

- [41] T.O. Wehling, K.S. Novoselov, S.V. Morozov, E.E. Vdovin, M.I. Katsnelson, A.K. Geim, A.I. Lichtenstein, Molecular Doping of Graphene, *Nano Lett.* 8 (2008) 173–177. doi:10.1021/nl072364w.
- [42] S. Dou, A. Shen, L. Tao, S. Wang, Molecular doping of graphene as metal-free electrocatalyst for oxygen reduction reaction, *Chem. Commun.* 50 (2014) 10672. doi:10.1039/C4CC05055J.
- [43] M.S. Abdou, F.P. Orfino, Z.W. Xie, M.J. Deen, S. Holdcroft, Reversible charge transfer complexes between molecular oxygen and poly(3-alkylthiophene)s, *Adv. Mater.* 6 (1994) 838–841. <http://onlinelibrary.wiley.com/doi/10.1002/adma.19940061106/full> (accessed June 16, 2017).
- [44] Y. ying Wang, Z. hua Ni, T. Yu, Z.X. Shen, H. min Wang, Y. hong Wu, W. Chen, A.T. Shen Wee, Raman Studies of Monolayer Graphene: The Substrate Effect, *J. Phys. Chem. C.* 112 (2008) 10637–10640. doi:10.1021/jp8008404.
- [45] S. Das, D. Lahiri, A. Agarwal, W. Choi, Interfacial bonding characteristics between graphene and dielectric substrates, *Nanotechnology.* 25 (2014) 045707. doi:10.1088/0957-4484/25/4/045707.
- [46] Y.-J. Kang, J. Kang, K.J. Chang, Electronic structure of graphene and doping effect on SiO₂, *Phys. Rev. B.* 78 (2008). doi:10.1103/PhysRevB.78.115404.
- [47] Z. Cheng, Q. Zhou, C. Wang, Q. Li, C. Wang, Y. Fang, Toward Intrinsic Graphene Surfaces: A Systematic Study on Thermal Annealing and Wet-Chemical Treatment of SiO₂-Supported Graphene Devices, *Nano Lett.* 11 (2011) 767–771. doi:10.1021/nl103977d.
- [48] J.E. Lee, G. Ahn, J. Shim, Y.S. Lee, S. Ryu, Optical separation of mechanical strain from charge doping in graphene, *Nat. Commun.* 3 (2012) 1024. doi:10.1038/ncomms2022.
- [49] N.S. Mueller, S. Heeg, M.P. Alvarez, P. Kusch, S. Wasserroth, N. Clark, F. Schedin, J. Parthenios, K. Papagelis, C. Galiotis, M. Kalbáč, A. Vijayaraghavan, U. Hübner, R. Gorbachev, O. Frank, S. Reich, Evaluating arbitrary strain configurations and doping in graphene with Raman spectroscopy, *2D Mater.* 5 (2017) 015016. doi:10.1088/2053-1583/aa90b3.
- [50] A. Das, S. Pisana, B. Chakraborty, S. Piscanec, S.K. Saha, U.V. Waghmare, K.S. Novoselov, H.R. Krishnamurthy, A.K. Geim, A.C. Ferrari, A.K. Sood, Monitoring dopants by Raman scattering in an electrochemically top-gated graphene transistor, *Nat. Nanotechnol.* 3 (2008) 210–215. doi:10.1038/nnano.2008.67.
- [51] A. Das, B. Chakraborty, S. Piscanec, S. Pisana, A.K. Sood, A.C. Ferrari, Phonon renormalization in doped bilayer graphene, *Phys. Rev. B.* 79 (2009). doi:10.1103/PhysRevB.79.155417.
- [52] G. Froehlicher, S. Berciaud, Raman spectroscopy of electrochemically gated graphene transistors: Geometrical capacitance, electron-phonon, electron-electron, and electron-defect scattering, *Phys. Rev. B.* 91 (2015). doi:10.1103/PhysRevB.91.205413.
- [53] Y.-J. Kang, J. Kang, K.J. Chang, Electronic structure of graphene and doping effect on SiO₂, *Phys. Rev. B.* 78 (2008). doi:10.1103/PhysRevB.78.115404.
- [54] M.M. Fogler, D.S. Novikov, B.I. Shklovskii, Screening of a hypercritical charge in graphene, *Phys. Rev. B.* 76 (2007). doi:10.1103/PhysRevB.76.233402.
- [55] L. Bousse, N.F. De Rooij, P. Bergveld, Operation of chemically sensitive field-effect sensors as a function of the insulator-electrolyte interface, *IEEE Trans. Electron Devices.* 30 (1983) 1263–1270.
- [56] Fung C.D., Cheung P.W., Ko W.H., A generalized theory of an electrolyte-insulator-semiconductor field-effect transistor, *IEEE Trans. Electron Devices.* 33 (1986) 8–18.
- [57] M. Nonnenmacher, M.P. O’Boyle, H.K. Wickramasinghe, Kelvin probe force microscopy, *Appl. Phys. Lett.* 58 (1991) 2921–2923. doi:10.1063/1.105227.
- [58] V. Panchal, R. Pearce, R. Yakimova, A. Tzalenchuk, O. Kazakova, Standardization of surface potential measurements of graphene domains, *Sci. Rep.* 3 (2013). doi:10.1038/srep02597.

- [59] A.K. Henning, T. Hochwitz, J. Slinkman, J. Never, S. Hoffmann, P. Kaszuba, C. Daghljan, Two-dimensional surface dopant profiling in silicon using scanning Kelvin probe microscopy, *J. Appl. Phys.* 77 (1995) 1888–1896. doi:10.1063/1.358819.
- [60] C. Maragliano, S. Lilliu, M.S. Dahlem, M. Chiesa, T. Souier, M. Stefancich, Quantifying charge carrier concentration in ZnO thin films by Scanning Kelvin Probe Microscopy, *Sci. Rep.* 4 (2015). doi:10.1038/srep04203.
- [61] W.N. Hansen, G.J. Hansen, Standard reference surfaces for work function measurements in air, *Surf. Sci.* 481 (2001) 172–184. doi:10.1016/S0039-6028(01)01036-6.
- [62] O.A. Castañeda-Uribe, R. Reifenberger, A. Raman, A. Avila, Depth-Sensitive Subsurface Imaging of Polymer Nanocomposites Using Second Harmonic Kelvin Probe Force Microscopy, *ACS Nano.* 9 (2015) 2938–2947. doi:10.1021/nn507019c.
- [63] D. Pierucci, J.-J. Gallet, F. Bournel, F. Sirotti, M.G. Silly, H. Tissot, A. Naitabdi, F. Rochet, Real-Time X-ray Photoemission Spectroscopy Study of Si(001)-2×1 Exposed to Water Vapor: Adsorption Kinetics, Fermi Level Positioning, and Electron Affinity Variations, *J. Phys. Chem. C.* 120 (2016) 21631–21641. doi:10.1021/acs.jpcc.6b07360.
- [64] W. Mönch, Hydrogen-Modification of Electronic Surface, Bulk, and Interface Properties of Si, *Phys. Status Solidi A.* 159 (1997) 25–37. doi:10.1002/1521-396X(199701)159:1<25::AID-PSSA25>3.0.CO;2-C.
- [65] T. Hattori, Advanced Research Workshop on Fundamental Aspects of Ultrathin Dielectrics on Si-based Devices: Towards an Atomic-Scale Understanding, 1998.
- [66] T. Hattori, Surface, interface and valence band structures of ultra-thin silicon oxides, *Appl. Surf. Sci.* 130–132 (1998) 156–164. doi:10.1016/S0169-4332(98)00043-9.
- [67] H. Nohira, A. Omura, M. Katayama, T. Hattori, Valence band edge of ultra-thin silicon oxide near the interface, *Appl. Surf. Sci.* 123–124 (1998) 546–549. doi:10.1016/S0169-4332(97)00568-0.
- [68] P.V. Avramov, A.A. Kuzubov, A.S. Fedorov, P.B. Sorokin, F.N. Tomilin, Y. Maeda, Density-functional theory study of the electronic structure of thin Si/SiO₂ quantum nanodots and nanowires, *Phys. Rev. B.* 75 (2007). doi:10.1103/PhysRevB.75.205427.